THE JOURNAL OF PHYSICAL CHEMISTRY C

pubs.acs.org/JPCC Article

Water Slippage on Graphitic and Metallic Surfaces: Impact of the Surface Packing Structure and Electron Density Tail

Kang Jin Cho, Suji Gim, Hyung-Kyu Lim, Changho Kim,* and Hyungjun Kim*

Cite This: J. Phys. Chem. C 2020, 124, 11392−11400 Read Online

ACCESS | Metrics & More | Article Recommendations | Supporting Information

ABSTRACT: While fluid flow at solid−liquid interfaces has been of great interest, studying its behavior is challenging because it requires a comprehensive understanding of the complex interactions that exist at various realistic solid−liquid interfaces. In particular, the slip phenomenon had been a debated subject for decades before the phenomenon was proven at a molecular level. Since the slip behavior is widely acknowledged, its fundamental relationships with other measurable physical properties have been studied intensively. Here, we present a first-principles-based multiscale simulation study on various solid−water interfacial systems to understand how the physical quantities influence the slip length. Based on the simulation results, we propose an extended quasi-universal relationship between the slip length and the work of adhesion by considering the surface packing density. Furthermore, we scrutinize the effects of the electron density tail from the solid wall on both the slip length and work of adhesion. We also investigate the relationship between the self-diffusivity of the fluid at the interface and the slip length. Our present study underlines the impact of atomic-level details of the solid−liquid interfaces, such as the surface packing structure and electrostatic interactions, on determining the hydrodynamic boundary conditions.

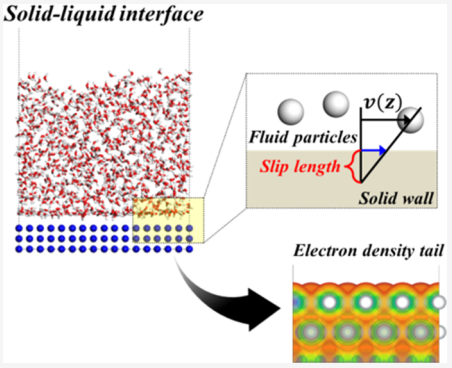

1. INTRODUCTION

Dynamics of liquids confined by solid walls has been studied for several decades.[1−3] Due to the different characteristics of a liquid on a solid wall and bulk liquid, the importance of understanding the fluidic motion at the solid−liquid boundary has been acknowledged in the fields of biology, microelectronics, nanoscale electromechanical systems, and lab-on-a-chip devices, to name a few.[4−7] From the microscopic point of view, transport phenomena are significantly affected by the intermolecular interactions at the solid−liquid interface,[8,9] which promotes many studies on the chemophysical properties of the fluid at the molecular level to fundamentally understand the transport phenomena in the solid−liquid interfacial region.

When the fluid dynamics is described using macroscopic fluid dynamic equations, a no-slip boundary condition at the solid wall is assumed usually for the sake of convenience.[1,10] However, from a number of computational simulations and experimental measurements,[11−14] it has been shown that the liquid molecules on the motionless solid surface can indeed slip with a nonzero slip velocity. Therefore, by quantifying the degree of liquid slippage on the solid wall through the slip velocity or slip length (Figure 1), a theoretical link between the microscopic interfacial characteristics and the macroscopic flow parameters can be established.

Extensive studies have been conducted to establish connections between the slip length, b, and other fundamental physical properties of the solid−liquid interface.[15,16] In particular, a quasi-universal relation between b and the surface wettability has been suggested.[17] This was justified by considering the proportionality of the solid−liquid friction coefficient, κ (inversely proportional to b), to the square of the solid−liquid attraction energy scale, ϵ_{sl}

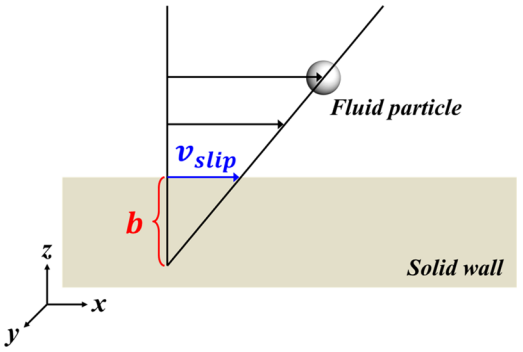

Figure 1. Slip length (b) and slip velocity (v_{slip}) at the solid−liquid interface in the case of slip flow.

Received: January 31, 2020
Revised: May 1, 2020
Published: May 1, 2020

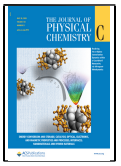

https://dx.doi.org/10.1021/acs.jpcc.0c00854
J. Phys. Chem. C 2020, 124, 11392−11400

$$b = \frac{\eta}{\kappa} \propto \varepsilon_{sl}^{-2} \tag{1}$$

with η being the shear viscosity of the liquid. Since ε_{sl} can be represented using the solid−liquid work of adhesion, W_{ad}, the Young−Dupré equation redictates eq 1 in terms of an experimentally measurable contact angle, θ_c

$$b \propto W_{ad}^{-2} \propto (1 + \cos\theta_c)^{-2} \tag{2}$$

However, the validity of such a quasi-universal correlation is still questionable. Although experiments have demonstrated that the amount of slip usually shows a trend to increase with θ_c,[18] it was reported that this correlation is not clearly observed for polar solvents.[19] In addition, a collection of various experimental reports also demonstrated a poor correlation between b and θ_c.[20]

Here, we investigate the slip length dependency on the surface wettability using computational approaches. To develop a clear understanding of the water slippage in realistic systems, we employ our recently developed mean-field quantum mechanics/molecular mechanics (QM/MM) simulation method, coined as DFT-CES (density functional theory in classical explicit solvents),[21] which can reflect full details of the atomic arrangements and electron density tails of metallic surfaces. By calculating the slip length, b, and the work of adhesion, W_{ad}, for water at various graphitic and metal surfaces, we investigate the validity of the quasi-universal correlation between b and W_{ad} and other factors affecting b in realistic systems.

2. COMPUTATIONAL DETAILS

2.1. Slip Length Calculation from Equilibrium Molecular Dynamics Simulations. The slip length, b, is defined as an extrapolated distance into the solid wall where the fluid velocity vanishes (Figure 1). Consequently, a straightforward method to compute b is to perform non-equilibrium molecular dynamics (NEMD) simulations by generating Poiseuille flow or Couette flow and measuring the streaming velocity profile. However, the arbitrariness in determining the external field strength in nanoscale simulations invokes practical issues and uncertainties in calculating b from NEMD.[22]

For a Newtonian fluid with a viscous friction model, the constitutive equation leads to $b = \eta/\kappa$. Here, the shear viscosity, η, is the fluid characteristic that can be obtained from the stress autocorrelation function via the Green−Kubo (GK) relation using equilibrium molecular dynamics (EMD) simulations. Therefore, to compute b from EMD, one needs to formulate another GK-like relation for the solid−liquid friction coefficient, κ. In their seminal work, Bocquet and Barrat (BB) suggested a GK-like expression for κ, which was derived using the linear-response theory (LRT).[23] However, several criticisms were raised in the application of the BB method in relation to the convergence of the integral and its accuracy.[24] More recently, Huang and Szlufarska (HS) developed an improved method based on the generalized Langevin equation (GLE).[25] In their method, κ is defined by summing up the contributions from individual fluid particles located near the interface, which is normalized by the surface area, A: $\kappa = \frac{\sum_i \kappa_i}{A}$ (with i being the index for the fluid particles). Then, the friction coefficient of an individual particle, κ_i, is formulated using LRT and GLE. This leads to the final expression for κ in terms of the autocorrelation function of the surface-parallel component of the force exerted on the ith liquid molecule by the solid wall, $F_{x,i}$

$$\kappa = \frac{\sum_i \int_0^\infty \langle F_{x,i}(0) F_{x,i}(t)\rangle \mathrm{d}t}{A k_B T[1 - \alpha]} \tag{3}$$

Here, we choose the surface-normal direction as the z-direction and the xy-plane as the surface-parallel plane. This leads to $\langle F_{x,i}(0)F_{x,i}(t)\rangle = \langle F_{y,i}(0)F_{y,i}(t)\rangle$ considering the system symmetry, and α in eq 3 is defined as

$$\alpha = \frac{1}{k_B T} \int_0^\infty \langle F_{x,i}(0) v_{x,i}(t)\rangle \mathrm{d}t \tag{4}$$

where $v_{x,i}$ is the surface-parallel component of the velocity of the ith liquid molecule.

Although the summation in eq 3 needs to be carried out over the fluid particles near the interface, it can be simply approximated as the summation over all fluid particles in the simulation cell since $F_{x,i}$ vanishes when the liquid molecule is located far from the solid surface.

Ramos-Alvarado et al. recently performed a careful comparison among various equilibrium models of the hydrodynamic slip as well as NEMD simulations.[26] They found that the HS method not only provides more numerically reliable values than other GK-like formalisms for κ but also yields consistent values with the NEMD results in the limit of a small external field, i.e., in the linear-response regime. In this study, we thus employ the GK expression, eq 3, proposed by Huang and Szlufarska to compute the friction coefficient, κ, which is converted into the slip length, b.

2.2. Multiscale Simulation and Wettability Prediction. For a realistic description of the nonbonding interaction between water and solid surfaces, an accurate description of electrostatic and van der Waals (vdW) interactions in the interfacial region is critical. Particularly, for metals, the electrostatic interaction originates from the surface polarization of the solid electrons and the detailed shape of the electron density tail, which cannot accurately be described using a fixed-point charge model. In this study, we thus use our recently developed multiscale simulation method, DFT-CES.[21] To simulate solid−liquid interfaces, we employ the quantum mechanical description of the solid and the classical description of the liquid.[27,28] Although full details of DFT-CES can be found in our previous papers,[21,29] we outline the key features of DFT-CES as follows.

1. The DFT-CES method is based on a mean-field coupling between the quantum mechanics (QM) region and the molecular mechanics (MM) region.
2. DFT and classical MD simulations are performed iteratively until the self-consistent solution is obtained; ensemble (or time)-averaged classical charge distribution sampled from the previous MD run is applied as an external potential for DFT optimization to polarize electron density, whereas the electrostatic potential from the DFT-optimized electron density and nuclei is applied as an external potential for classical particles during the subsequent MD run.
3. The electrostatic interaction between QM and MM regions is mediated using a real-space grid with a fine mesh size, which can represent full details of the electron density shape of the solid QM part (without a partial

https://dx.doi.org/10.1021/acs.jpcc.0c00854
J. Phys. Chem. C 2020, 124, 11392−11400

charge fitting scheme, such as an electrostatic potential fitting).

Notably, in our previous studies, we successfully employed our DFT-CES method to investigate the surface wettability of various solid surfaces.[27,28] We quantified the work of adhesion, W_{ad}, by calculating the free energy difference before and after the water slab contacts the solid surface using the two-phase thermodynamic (2PT) method.[30,31] By systematically parameterizing the vdW interaction between the QM and MM regions in a first-principles-based manner (without involving an empirical fitting), we obtained the values of W_{ad} quantitatively comparable to the experimental results for the graphitic[27] and metal surfaces.[28] The values are summarized in Table 1.

Table 1. Calculated Work of Adhesion (W_{ad}) Values for the Graphitic and Metallic Surfaces[a27,28]

	W_{ad} (mJ/m^2)
Ag(111)	195.2
Au(111)	219.1
Pd(111)	324.7
Pt(111)	265.1
Ag(100)	179.1
Au(100)	199.5
Pd(100)	301.6
Pt(100)	255.5
monolayer graphene (Gr-1)	98.5
bilayer graphene (Gr-2)	109.5
trilayer graphene (Gr-3)	111.5
graphite (Gr-8)	111.9

[a]The vdW parameters used in the DFT-CES simulations can be found from refs 27, 28.

2.3. Simulation Details. We investigate water slippage on graphitic surfaces for a monolayer, bilayer, and trilayer of graphene and on a graphite that is modeled using eight layers of graphene. We also investigate water slippage on the (111) and (100) surfaces of Ag, Au, Pd, and Pt metals. Using DFT-CES, we model the solid surface with its electron density at the QM level (which enables us to include the electrostatic interaction) while treating the fluid classically.

To simulate the QM region, we used the Quantum ESPRESSO[32] program (a planewave DFT code). We chose the Perdew–Burke–Ernzerhof (PBE) correlation functional[33] to describe the exchange–correlation energy of DFT, and the projector-augmented wave (PAW) method to describe the electronic–ionic interactions. For the DFT part, the graphitic surfaces were simulated using $(2\sqrt{3} \times 3)$rect surface unit cells consisting of 24 carbon atoms for each layer with dimensions of 8.55 × 7.40 Å^2. The (111) metallic surfaces were simulated using a three-layer slab with $(2\sqrt{3} \times 4)$rect surface unit cells with dimensions of 10.16 × 11.73 Å^2 (for Ag), 10.22 × 11.81 Å^2 (Au), 9.68 × 11.17 Å^2 (Pd), and 9.77 × 11.28 Å^2 (Pt). The (100) metallic surfaces were simulated using a three-layer slab with (2 × 2) surface unit cells with dimensions of 8.29 × 8.29 Å^2 (Ag), 8.31 × 8.31 Å^2 (Au), 7.88 × 7.88 Å^2 (Pd), and 7.94 × 7.94 Å^2 (Pt). The kinetic energy cutoff was set to 50 Ry, and a Monkhorst–Pack 5 × 5 × 1 grid in the case of graphitic surfaces and a 4 × 4 × 1 grid in the case of metal surfaces were applied in the reciprocal space. Also, the dipole correction was applied along the surface-normal z-direction.

To simulate classical fluids, we performed canonical ensemble MD simulations using the large-scale atomic/molecular massively parallel simulator (LAMMPS).[34] The snapshots of MD simulations are shown in Figure 2. For each surface, a total of 1000 classical TIP3P-Ew water molecules[35] were simulated using a Nosé–Hoover thermostat at 300 K

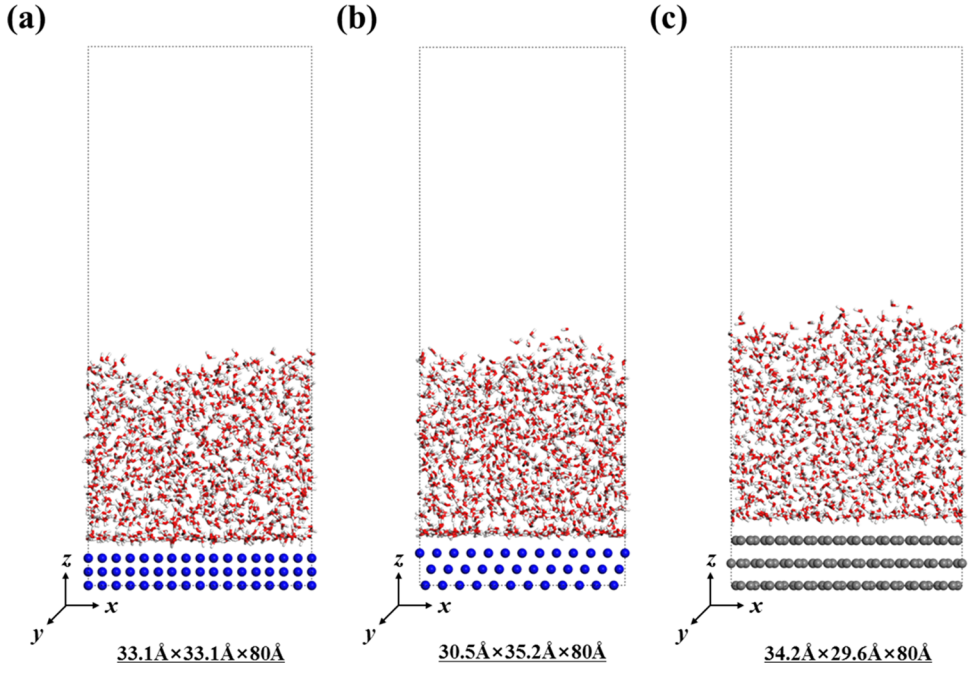

Figure 2. DFT-CES simulation cells for solid–liquid interfacial systems for the representative cases of (a) Ag(100) surface, (b) Ag(111) surface, and (c) trilayer graphene surface (Gr-3). Each system contains 1000 number of classical water molecules that are interfaced with the quantum mechanically described solid surface. Periodic boundary conditions were applied for the x-axis and y-axis, and an open boundary condition was applied for the z-axis.

https://dx.doi.org/10.1021/acs.jpcc.0c00854
J. Phys. Chem. C 2020, 124, 11392–11400

with a damping parameter of 100 fs. We applied periodic boundary conditions for the x- and y-directions and an open boundary condition for the z-direction. To treat the long-range electrostatic interaction in the simulation cells with mixed boundary conditions, we used the multilevel summation method (MSM).[36] The external potential from the QM region was set as follows. For the graphitic surface, the DFT-optimized structure and the electron density obtained from the $(2\sqrt{3} \times 3)$rect surface unit cells were repeated to fill the $(8\sqrt{3} \times 12)$rect surface unit cells. Similarly, the $(6\sqrt{3} \times 12)$ rect surface unit cells were filled by repeating the $(2\sqrt{3} \times 4)$rect surface unit cells for the (111) metallic surfaces, whereas the (8×8) cells were filled by the (2×2) cells for the (100) metallic surfaces. The dimensions of all simulation cells are given as follows: for graphitic surfaces, 34.2 × 29.6 × 80.0 Å^3; for the (111) surface, 30.5 × 35.2 × 80.0 Å^3 (Ag), 30.7 × 35.4 × 80.0 Å^3 (Au), 29.0 × 33.5 × 80.0 Å^3 (Pd), and 29.3 × 33.8 × 80.0 Å^3 (Pt); and for the (100) surfaces, 33.1 × 33.1 × 80.0 Å^3 (Ag), 33.2 × 33.2 × 80.0 Å^3 (Au), 31.5 × 31.5 × 80.0 Å^3 (Pd), and 31.7 × 31.7 × 80.0 Å^3 (Pt).

At every DFT-CES iteration, we performed an MD simulation for 1 ns and used the last 500 ps trajectory to calculate the average electrostatic potential, which was employed in the subsequent DFT calculation as an external potential. Once after the DFT-CES iteration was converged, we additionally performed 1 ns MD simulations to calculate the various parameters analyzed in this study.

3. RESULTS AND DISCUSSION

3.1. Water Slippage on Various Surfaces. In this section, we omit the particle index i (e.g., F_x and v_x). Note that $\langle F_{x,i}(0)F_{x,i}(t)\rangle$ does not depend on i.

From the final MD run of DFT-CES iterations for each surface, we calculated the autocorrelation function of F_x (FACF). We recall that F_x denotes the x-component of the force exerted on a liquid molecule by the wall. As representatively shown in Figure 3 for the Ag(100) and trilayer graphene surfaces (indicated as Gr-3), we find that the FACF sufficiently decays within 10 ps and thus the integral of FACF adequately converges to a specific value for that time scale. We also calculated the cross-correlation function of F_x and v_x (FVCCF) to obtain α using eq 4 (Figure S2). Consistent with the previous discussion,[25] we also find that $\alpha \ll 1$ for all cases investigated here; α is on the order of 10^{-2}–10^{-4} for the metallic surfaces and $<10^{-4}$ for the graphitic surfaces. From the integral of FACF and α, we compute the values of the solid–liquid friction coefficient (κ) using eq 3, which are listed in Table 2. Using η = 0.314 mPa·s determined from a separate MD simulation of the bulk TIP3P-Ew water (which is also consistent with previous results[37−39]), we also obtain the slip length values, $b = \eta/\kappa$ (Table 2).

For hydrophobic graphitic surfaces, we obtained fairly large slip lengths of 80–110 nm, which are consistent with the previous experimental results and other theoretical predictions ranging from 8 to 115 nm.[22,40,41] On the other hand, we obtained much smaller slip lengths of 0.1–0.5 nm for the hydrophilic metal surfaces, which can also be compared to the previous experimental value of 0.3 nm.[42] In between (111) and (100) surfaces, the slip length on the (111) plane is larger than that on the (100) plane for all four metal cases. This can be ascribed to the water molecules on a more densely packed surface, which can slip more smoothly. Thus, the slip length seemingly depends on the surface hydrophobicity and structure, which will be discussed in more detail below.

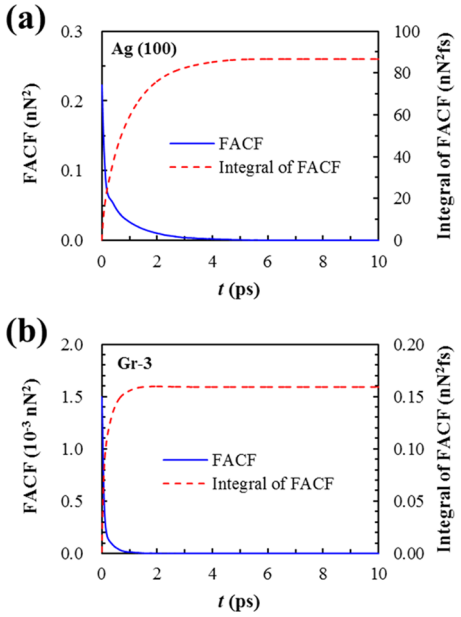

Figure 3. Force autocorrelation function (FACF) $\langle F_x(0)F_x(t)\rangle$ and its time integral for the interaction between a water molecule and the solid wall: (a) Ag(100) surface and (b) trilayer graphene surface (Gr-3). Two different y-axes are used for FACF (left) and time integral of FACF (right). Only the surface-parallel component (F_x) is considered when calculating the FACF. The time integral of FACF attains a convergent value within 10 ps.

Table 2. Calculated Friction Coefficient (κ) and Slip Length (b) Values for the Graphitic and Metal Surfaces[a]

	friction coefficient, κ ($\times 10^4$ kg/m^2 s)	slip length, b (nm)
Ag(111)	53.9	0.58
Au(111)	62.6	0.50
Pd(111)	235.6	0.13
Pt(111)	95.5	0.33
Ag(100)	191.8	0.16
Au(100)	204.0	0.15
Pd(100)	585.6	0.05
Pt(100)	302.8	0.10
monolayer graphene (Gr-1)	0.28	111.7
bilayer graphene (Gr-2)	0.37	85.2
trilayer graphene (Gr-3)	0.38	82.7
graphite (Gr-8)	0.39	80.3

[a]The slip length was calculated from the viscosity and friction coefficient, which are obtained from MD simulations.

3.2. Slip Length versus Work of Adhesion. To investigate the dependency of slip length on the surface hydrophobicity, we plot b values obtained from the various solid surfaces versus the inverse square of W_{ad}, based on eq 2. As shown in Figure 4, for each surface structure (i.e., closed-packed (111) surface and square-packed (100) surface), there exists a strong correlation between b and W_{ad}^{-2} among data points obtained from systems with different metals. In addition, for the honeycomb lattice of the graphitic surface, a similar correlation is observed among data points obtained from systems with different numbers of layers. However, the proportionality shows distinct differences depending on the

https://dx.doi.org/10.1021/acs.jpcc.0c00854
J. Phys. Chem. C 2020, 124, 11392−11400

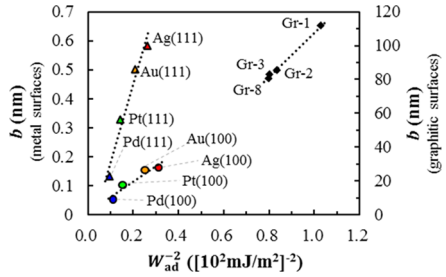

Figure 4. Correlation between the slip length (b) and W_{ad}^{-2} (inverse square of the work of adhesion). Two scales of the y-axis are used for metal surfaces (left) and graphitic surfaces (right). The proportionality between b and W_{ad}^{-2} varies for different surface packing structures.

surface structures. Hence, the surface wettability is not a unique physical parameter that determines the slip length.

We now trace the origin of different proportionality coefficients depending on the surface packing structures by relating the magnitudes of F_x and F_z to the slip length, b, and the work of adhesion, W_{ad}, respectively. Considering $\alpha \ll 1$, the friction coefficient, κ, is nearly proportional to the integral of FACF (see eq 3). By introducing a relaxation time scale, τ, for FACF, the integral of FACF can be understood as

$$\int_0^\infty \langle F_x(0)F_x(t)\rangle dt \approx \langle F_x^2\rangle \tau \tag{5}$$

As shown in Figure 5a, we find that the integral of FACF is roughly proportional to $\langle F_x^2\rangle$. Hence, these observations yield

$$b \propto \kappa^{-1} \propto \langle F_x^2\rangle^{-1} \tag{6}$$

On the other hand, W_{ad} is defined as the amount of work involved in detaching a water slab from the solid surface along the direction normal to the surface. We thus postulate

$$W_{ad} \propto \sqrt{\langle F_z^2\rangle} \tag{7}$$

which is numerically confirmed in our cases, as shown in Figure 5b.

Therefore, eqs 6 and 7 would result in the original relation of $b \propto W_{ad}^{-2}$ if the proportionality coefficient between $\langle F_x^2\rangle$ and $\langle F_z^2\rangle$ does not depend on the surface packing structures. However, as shown in Figure 5c, the proportionality strongly depends on the surface structures.

3.3. Modeling of Surface Packing Structure-Dependent Proportionality. Since F_x and F_z are the surface-parallel and surface-normal components of the force exerted by the solid wall on a single fluid particle, it is expected that the ratio of their magnitudes is primarily determined by the surface packing structure. Thus, here, we investigate the dependence of the proportionality constant, c, between $\sqrt{\langle F_x^2\rangle}$ and $\sqrt{\langle F_z^2\rangle}$ (i.e., $\sqrt{\langle F_x^2\rangle} = c\sqrt{\langle F_z^2\rangle}$) on the surface packing structure. For the sake of notational simplicity, we introduce lateral and orthogonal forces, $\boldsymbol{F}_\parallel = (F_x, F_y, 0)$ and $\boldsymbol{F}_\perp = (0, 0, F_z)$.

To model c in a simple form, we assume that the force exerted by the solid surface on a fluid particle is given as the sum of the pairwise forces between the particle and each atom in the solid wall. In addition, we assume that the former force, denoted by $\boldsymbol{F}$, is predominantly determined by the pairwise force between the fluid particle and the nearest solid atom. Figure 6 illustrates this situation, where several geometric

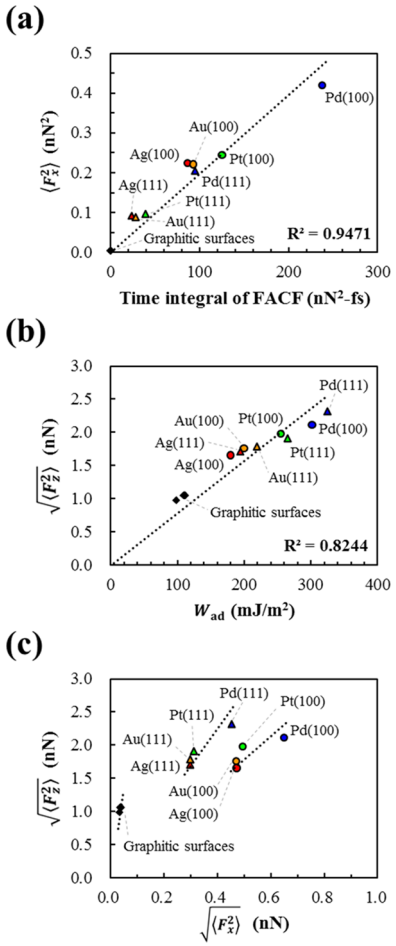

Figure 5. (a) Correlation between $\langle F_x^2\rangle$ and the integral of the force autocorrelation function (FACF) for the surface-parallel component (F_x). (b) Correlation between the square root of $\langle F_z^2\rangle$ and W_{ad}. (c) Correlation between the square root of $\langle F_z^2\rangle$ and the square root of $\langle F_x^2\rangle$, which shows different proportionality depending on the surface packing structures.

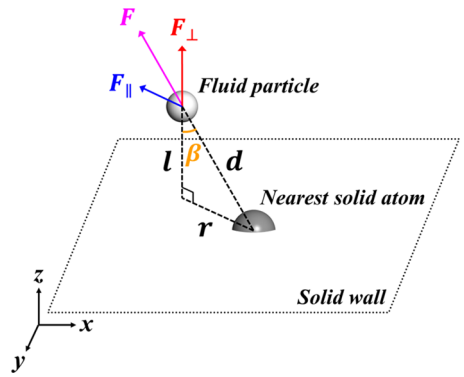

Figure 6. Graphical definition of geometric distances (d, l, and r) and an angle (β) when a single fluid particle experiences a pairwise force ($\boldsymbol{F}$) exerted by the nearest atom in the solid wall. The vector quantity of $\boldsymbol{F}$ can be decomposed into lateral and orthogonal vectors of $\boldsymbol{F}_\parallel = (F_x, F_y, 0)$ and $\boldsymbol{F}_\perp = (0, 0, F_z)$.

distances are defined; the distance between the fluid particle and the nearest solid atom is d, the distance between the fluid particle and the solid surface is l, and the distance between the nearest solid atom and the projected position of the fluid

https://dx.doi.org/10.1021/acs.jpcc.0c00854
J. Phys. Chem. C 2020, 124, 11392−11400

particle to the solid surface is $r \equiv \sqrt{d^2 - l^2}$. By introducing the angle β between the vectors associated with d and l (see Figure 6), we express the magnitudes of the lateral and orthogonal forces as $|F_{\parallel}| = |F| \sin\beta$ and $|F_{\perp}| = |F| \cos\beta$, respectively, and thus, $|F_{\parallel}|/|F_{\perp}| = \tan\beta = r/l$. Since $|F_{\parallel}| = =\sqrt{F_x^2 + F_y^2}$, $|F_{\perp}| = \sqrt{F_z^2}$, and $\langle F_x^2 \rangle = \langle F_y^2 \rangle$ due to the system symmetry, we relate the proportionality coefficient c with r and l. That is, $c = \sqrt{F_x^2}/\sqrt{F_z^2} = \sqrt{F_{\parallel}^2}/\sqrt{2F_{\perp}^2} \approx |F_{\parallel}|/(\sqrt{2}|F_{\perp}|) = r/(\sqrt{2}l)$.

It is noted that for a fixed value of l (i.e., a fluid particle separated from the solid surface by distance l), the ratio c is a function of r where the range of r is bounded by the length scale of the interparticle separation on the solid wall. For the surface packing density (n_s) of the solid wall, the interparticle separation length scale is given as $n_s^{-1/2}$. Hence, by further assuming that r has a uniform distribution on the interval $[0, n_s^{-1/2}]$, we express the average value of c as

$$c = \int_0^{n_s^{-1/2}} c(r) 2\pi r dr \propto n_s^{-3/2} \tag{8}$$

We thus postulate the relation $\sqrt{F_x^2} \propto n_s^{-3/2}\sqrt{F_z^2}$, which is numerically confirmed, as shown in Figure S3. By combining this result with eqs 6, 7 and 8, we finally obtain

$$n_s^{-3} b \propto W_{ad}^{-2} \tag{9}$$

A comparison between Figure 7a,b shows that the inclusion of correction factor n_s^{-3} to b significantly improves the quality of its correlation with W_{ad}^{-2} ($R^2 = 0.9125$). Considering that eq 9 is obtained from simplifying assumptions, this improvement is remarkable. When n_s^m is used with an empirically chosen exponent $m = -3.9$, the correlation is observed to be further improved (see Figure 7c).

We thus conclude that, besides the surface wettability, another important factor that affects the slip length is the surface packing density, which yields the generalized relation, eq 9. However, we also note that more expanded studies for many different types of crystal structures would be required to quantitatively confirm the universality of the empirically chosen exponent m in the future.

3.4. Other Factors Affecting the Slip Length: Electron Density Tail and Self-Diffusivity at the Interface. Since DFT-CES accurately models the electrostatic interaction between the fluid particles and the electron density tail of the solid, we further investigate the effect of the electrostatic interaction on the water slippage on various solid surfaces. By switching on and off the electrostatic interaction created by the nuclei and electrons of the QM solid, we obtain the values of b and W_{ad} (see Figure 8). It is observed that the electrostatic interaction increases the friction on the metallic surfaces (Figure 8a,b) whereas it reduces the friction on the graphitic surfaces (Figure 8c). Hence, the electrostatic interaction substantially modifies b but in an opposite manner for the metallic and graphitic surfaces.

For metallic surfaces, the electrostatic contribution is significant and increases the $\langle F_x^2 \rangle$ by an approximate factor of 1.5. Additionally, the electrostatic contribution also increases τ by up to ~50% (Table S1). Therefore, by recalling eq 5, the integral of FACF increases due to the existence of the electrostatic interaction, which substantially increases the friction. We conceive that the change in τ is due to the fact

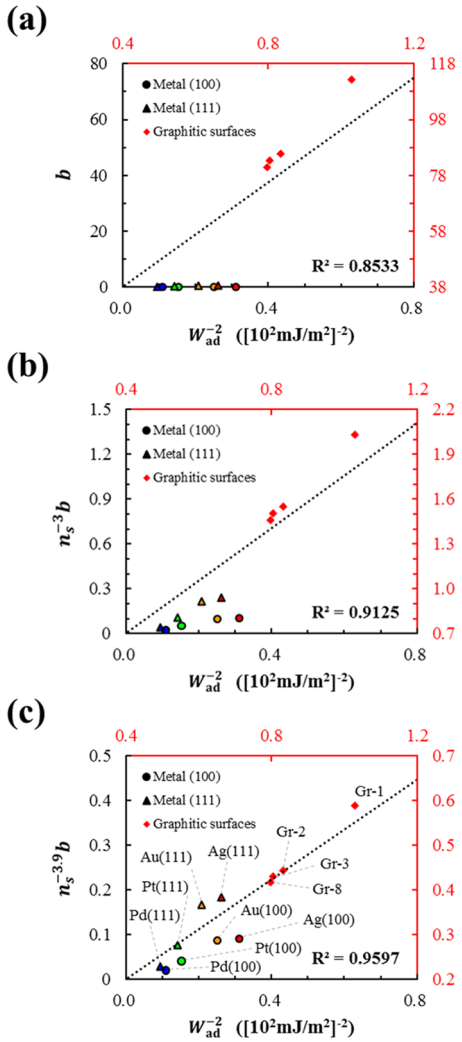

Figure 7. (a) Original quasi-universal relation between b and W_{ad}^{-2}, (b) revised relation between $n_s^{-3}b$ and W_{ad}^{-2}, and (c) revised relation between $n_s^{-3.9}b$ and W_{ad}^{-2}. Note that the exponent −3.9 in (c) is empirically chosen. The black axes are designated for the metal (100) and (111) surfaces, and the red axes are designated for the graphitic surfaces. The dotted lines are trend lines from all data points. The corresponding surface of each data point can be found in (c).

that the liquid-particle dynamics with and without the electrostatic interaction is noticeably different, which affects the associated relaxation time scales. For graphitic surfaces, the electrostatic contribution is rather auxiliary, while the vdW contribution mostly determines the solid−liquid interaction. Indeed, the existence of the ES interaction marginally decreases $\langle F_x^2 \rangle$ to less than 5% (Table S1). However, by turning on the electrostatic interaction, liquid particles can experience the effect of the complex shape of the electrostatic field created by the p_z orbitals of carbon atoms. This electrostatic contribution expedites the memory loss of F_x, which shortens τ, and thus decreases the friction.

On the other hand, we find that the sensitivity of W_{ad} to the existence of the electrostatic interaction is much weaker. It is thus inferred that the detailed shape of the electron density tail of the solid, which has little impact on the surface wettability, is important in determining the hydrodynamic boundary conditions.

https://dx.doi.org/10.1021/acs.jpcc.0c00854
J. Phys. Chem. C 2020, 124, 11392−11400

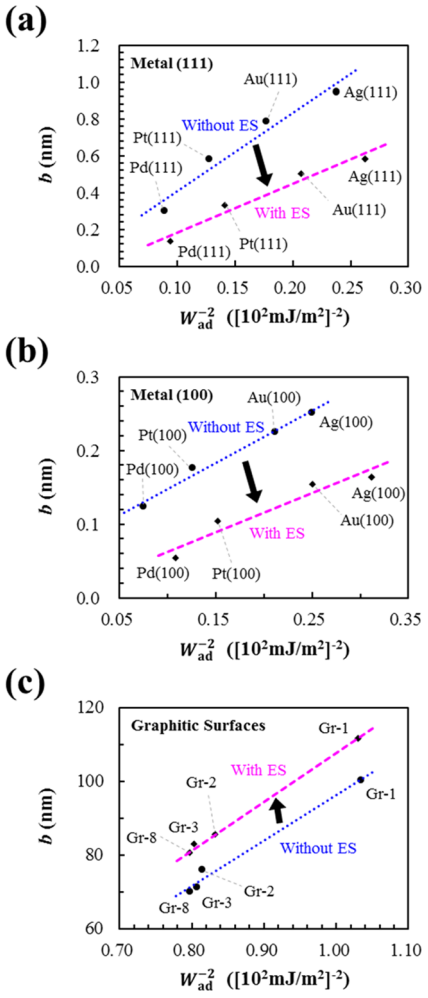

Figure 8. Effect of the electron density tail on b and W_{ad} in the cases of (a) metal (111) surfaces, (b) metal (100) surfaces, and (c) graphitic surfaces. The blue-dotted lines are for the cases without the electrostatic (ES) interaction, whereas the magenta-dashed lines are for the cases with the ES interaction. The inclusion of ES interaction largely modifies b, while it marginally changes W_{ad}, implying the importance of the ES interaction in determining b.

Another factor we investigate is the lateral self-diffusivity, $D_{||}$, of the fluid at the interface.[43] The value of $D_{||}$ is computed as follows. Since the density profile along the direction normal to the surface indicates the formation of a high-density region at the interface (Figure S4),[28] we quantified $D_{||}$ by computing the mean-squared displacement (MSD) of a water molecule that started its diffusion in this adlayer region, or by computing the velocity autocorrelation function (VACF) of a water molecule initially located in the adlayer region. We note that the values obtained from MSD and VACF agree well (Figure S5).

As shown in Figure 9a, while a strong correlation between b and $D_{||}$ is observed for each surface structure, we find that the proportionality shows distinct differences depending on the surface packing structure. We note that this observation is similar to the case between b and W_{ad}^{-2}. In fact, considering a strong correlation between W_{ad}^{-2} and $D_{||}$, the proportionality of which is observed not to depend on the surface packing structure (see Figure 9b), the surface structure-dependent proportionality between b and $D_{||}$ is expected from the surface structure-dependent proportionality between b and W_{ad}^{-2}. The behavior of b, W_{ad}^{-2}, and $D_{||}$ can be understood from the

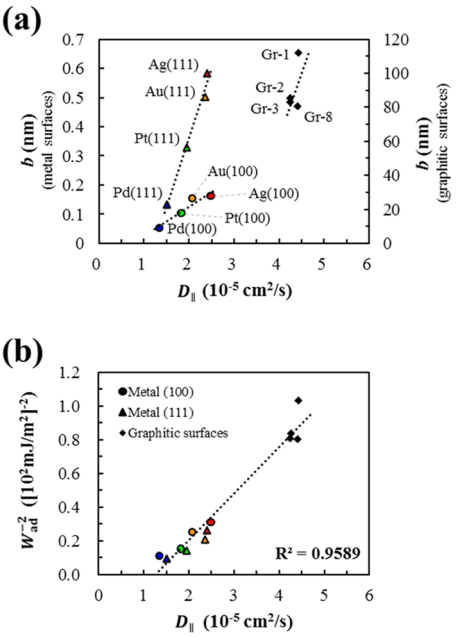

Figure 9. (a) Correlation between the slip length (b) and the surface-parallel diffusion coefficient ($D_{||}$). (b) Correlation between W_{ad}^{-2} (inverse square of the work of adhesion) and $D_{||}$. Since $D_{||}$ strongly correlates with W_{ad}^{-2}, it shows different proportionality with b similar to W_{ad}^{-2}.

disparate characteristics between the friction by the solid surface that determines b and the friction by other fluid molecules that predominantly determines the self-diffusivity of dense fluids such as liquid water. As the solid−fluid interaction strength increases (i.e., as W_{ad} becomes larger), the local density of the fluid at the interface increases (Figure S6), yielding larger friction by the other fluid molecules and thus a smaller value of $D_{||}$. This leads to the strong correlation between W_{ad}^{-2} and $D_{||}$ and the surface structure-dependent proportionality between b and $D_{||}$.

4. CONCLUSIONS

In this study, we investigated how the hydrodynamic boundary condition is affected by various physical properties at the solid−liquid interface. We employed a multiscale simulation method recently developed by our group, DFT-CES, to accurately describe the interfacial interactions, including vdW and electrostatic interactions. We investigated the quasi-universal relationship between the slip length and the work of adhesion and found that the proportionality coefficient depends on the surface packing structures. By analyzing its origin, we proposed a revised quasi-universal relationship, where the surface packing density is further included to account for the effect of packing structures.

Furthermore, we examined the effect of the electron density tail and self-diffusivity of water at the interface on the hydrodynamic boundary condition. We found that the consideration of the high-order multipole electrostatic interaction due to the complex electron density tail significantly alters the slip length, while it marginally modifies the work of adhesion. We further found that the self-diffusivity of the fluid at the interface, which has also been discussed as a physical quantity that influences the slip length, is directly related to the work of adhesion rather than the slip length. This indicates that various factors affecting the hydrodynamic

https://dx.doi.org/10.1021/acs.jpcc.0c00854
J. Phys. Chem. C 2020, 124, 11392−11400

boundary condition cannot be simply encoded in a single physical quantity, such as the contact angle or the self-diffusivity at the interface.

We thus anticipate that computational simulations including detailed interfacial interactions will be essential for a comprehensive understanding of the solid−liquid interfacial properties and that our current simulation study, where the complex interfacial interactions are adequately modeled, will provide a new insight into the hydrodynamic boundary condition at various realistic solid−liquid interfaces.

■ ASSOCIATED CONTENT

Supporting Information

The Supporting Information is available free of charge at https://pubs.acs.org/doi/10.1021/acs.jpcc.0c00854.

Force−velocity cross-correlation function and α values, force component magnitude comparison, water density profiles, comparison of diffusion constants, and comparison between the adlayer density and the work of adhesion (PDF)

■ AUTHOR INFORMATION

Corresponding Authors

Changho Kim − *Department of Applied Mathematics, University of California, Merced, California 95343, United States*; Phone: +1-209-228-3388; Email: ckim103@ucmerced.edu

Hyungjun Kim − *Department of Chemistry and Graduate School of EEWS, Korea Advanced Institute of Science and Technology (KAIST), Daejeon 34141, Korea*; orcid.org/0000-0001-8261-9381; Phone: +82-42-350-1725; Email: linus16@kaist.ac.kr

Authors

Kang Jin Cho − *Department of Chemistry and Graduate School of EEWS, Korea Advanced Institute of Science and Technology (KAIST), Daejeon 34141, Korea*

Suji Gim − *Department of Chemistry and Graduate School of EEWS, Korea Advanced Institute of Science and Technology (KAIST), Daejeon 34141, Korea*

Hyung-Kyu Lim − *Division of Chemical Engineering and Bioengineering, Kangwon National University, Chuncheon, Gangwon-do 24341, Korea*; orcid.org/0000-0002-2403-2766

Complete contact information is available at: https://pubs.acs.org/10.1021/acs.jpcc.0c00854

Notes

The authors declare no competing financial interest.

■ ACKNOWLEDGMENTS

This work was supported by the Nanomaterial Technology Development Program (2019M3A7B4064417) of the National Research Foundation of Korea (NRF) and a grant funded by the Korean Government (MSIT) (NRF-2017R1A5A1015365).

■ REFERENCES

(1) Ruckenstein, E.; Rajora, P. On the no-slip boundary condition of hydrodynamics. *J. Colloid Interface Sci.* **1983**, *96*, 488−491.

(2) Bocquet, L.; Barrat, J. L. Hydrodynamic boundary conditions and correlation functions of confined fluids. *Phys. Rev. Lett.* **1993**, *70*, 2726−2729.

(3) Cottin-Bizonne, C.; Cross, B.; Steinberger, A.; Charlaix, E. Boundary slip on smooth hydrophobic surfaces: Intrinsic effects and possible artifacts. *Phys. Rev. Lett.* **2005**, *94*, No. 056102.

(4) Han, J.; Craighead, H. G. Separation of long DNA molecules in a microfabricated entropic trap array. *Science* **2000**, *288*, 1026−1029.

(5) de Groot, B. L.; Grubmuller, H. The dynamics and energetics of water permeation and proton exclusion in aquaporins. *Curr. Opin. Struct. Biol.* **2005**, *15*, 176−183.

(6) Erbas, N.; Baysal, O. Micron-level actuators for thermal management of microelectronic devices. *Heat Transfer Eng.* **2009**, *30*, 138−147.

(7) Sparreboom, W.; van den Berg, A.; Eijkel, J. C. Principles and applications of nanofluidic transport. *Nat. Nanotechnol.* **2009**, *4*, 713−720.

(8) Whitesides, G. M. The origins and the future of microfluidics. *Nature* **2006**, *442*, 368−373.

(9) Kobryn, A. E.; Kovalenko, A. Molecular theory of hydrodynamic boundary conditions in nanofluidics. *J. Chem. Phys.* **2008**, *129*, No. 134701.

(10) Richardson, S. On the no-slip boundary condition. *J. Fluid Mech.* **1973**, *59*, 707−719.

(11) Thompson, P. A.; Troian, S. M. A general boundary condition for liquid flow at solid surfaces. *Nature* **1997**, *389*, 360−362.

(12) Barrat, J. L.; Bocquet, L. Large slip effect at a nonwetting fluid-solid interface. *Phys. Rev. Lett.* **1999**, *82*, 4671−4674.

(13) Pit, R.; Hervet, H.; Leger, L. Direct experimental evidence of slip in hexadecane: Solid interfaces. *Phys. Rev. Lett.* **2000**, *85*, 980−983.

(14) Ortiz-Young, D.; Chiu, H. C.; Kim, S.; Voitchovsky, K.; Riedo, E. The interplay between apparent viscosity and wettability in nanoconfined water. *Nat. Commun.* **2013**, *4*, No. 2482.

(15) Cottin-Bizonne, C.; Barrat, J. L.; Bocquet, L.; Charlaix, E. Low-friction flows of liquid at nanopatterned interfaces. *Nat. Mater.* **2003**, *2*, 237−240.

(16) Voronov, R. S.; Papavassiliou, D. V.; Lee, L. L. Boundary slip and wetting properties of interfaces: Correlation of the contact angle with the slip length. *J. Chem. Phys.* **2006**, *124*, No. 204701.

(17) Huang, D. M.; Sendner, C.; Horinek, D.; Netz, R. R.; Bocquet, L. Water slippage versus contact angle: A quasiuniversal relationship. *Phys. Rev. Lett.* **2008**, *101*, No. 226101.

(18) Zhu, Y.; Granick, S. Rate-dependent slip of Newtonian liquid at smooth surfaces. *Phys. Rev. Lett.* **2001**, *87*, No. 096105.

(19) Cho, J.-H. J.; Law, B. M.; Rieutord, F. Dipole-dependent slip of Newtonian liquids at smooth solid hydrophobic surfaces. *Phys. Rev. Lett.* **2004**, *92*, No. 166102.

(20) Lauga, E.; Brenner, M.; Stone, H. In *Springer Handbook of Experimental Fluid Mechanics*; Tropea, C.; Yarin, A. L.; Foss, J. F., Eds.; Springer: Berlin, 2007; pp 1219−1240.

(21) Lim, H. K.; Lee, H.; Kim, H. A seamless grid-based interface for mean-field QM/MM coupled with efficient solvation free energy calculations. *J. Chem. Theory Comput.* **2016**, *12*, 5088−5099.

(22) Kumar Kannam, S.; Todd, B. D.; Hansen, J. S.; Daivis, P. J. Slip length of water on graphene: Limitations of non-equilibrium molecular dynamics simulations. *J. Chem. Phys.* **2012**, *136*, No. 024705.

(23) Bocquet, L.; Barrat, J. L. Hydrodynamic boundary conditions, correlation functions, and Kubo relations for confined fluids. *Phys. Rev. E* **1994**, *49*, 3079−3092.

(24) Petravic, J.; Harrowell, P. On the equilibrium calculation of the friction coefficient for liquid slip against a wall. *J. Chem. Phys.* **2007**, *127*, No. 174706.

(25) Huang, K.; Szlufarska, I. Green-Kubo relation for friction at liquid-solid interfaces. *Phys. Rev. E* **2014**, *89*, No. 032119.

(26) Ramos-Alvarado, B.; Kumar, S.; Peterson, G. P. Hydrodynamic slip length as a surface property. *Phys. Rev. E* **2016**, *93*, No. 023101.

(27) Gim, S.; Lim, H. K.; Kim, H. Multiscale simulation method for quantitative prediction of surface wettability at the atomistic level. *J. Phys. Chem. Lett.* **2018**, *9*, 1750−1758.
(28) Gim, S.; Cho, K. J.; Lim, H. K.; Kim, H. Structure, dynamics, and wettability of water at metal interfaces. *Sci. Rep.* **2019**, *9*, No. 14805.
(29) Lee, H.; Lim, H. K.; Kim, H. Hydration thermodynamics of non-polar aromatic hydrocarbons: Comparison of implicit and explicit solvation models. *Molecules* **2018**, *23*, No. 2927.
(30) Lin, S. T.; Maiti, P. K.; Goddard, W. A., III Two-phase thermodynamic model for efficient and accurate absolute entropy of water from molecular dynamics simulations. *J. Phys. Chem. B* **2010**, *114*, 8191−8198.
(31) Pascal, T. A.; Lin, S. T.; Goddard, W. A., III Thermodynamics of liquids: Standard molar entropies and heat capacities of common solvents from 2PT molecular dynamics. *Phys. Chem. Chem. Phys.* **2011**, *13*, 169−181.
(32) Giannozzi, P.; Baroni, S.; Bonini, N.; Calandra, M.; Car, R.; Cavazzoni, C.; Ceresoli, D.; Chiarotti, G. L.; Cococcioni, M.; Dabo, I.; et al. QUANTUM ESPRESSO: A modular and open-source software project for quantum simulations of materials. *J. Phys.: Condens. Matter* **2009**, *21*, No. 395502.
(33) Perdew, J. P.; Burke, K.; Ernzerhof, M. Generalized gradient approximation made simple. *Phys. Rev. Lett.* **1996**, *77*, 3865−3868.
(34) Plimpton, S. Fast parallel algorithms for short-range molecular dynamics. *J. Comput. Phys.* **1995**, *117*, 1−19.
(35) Price, D. J.; Brooks, C. L., III A modified TIP3P water potential for simulation with Ewald summation. *J. Chem. Phys.* **2004**, *121*, 10096−10103.
(36) Hardy, D. J.; Stone, J. E.; Schulten, K. Multilevel summation of electrostatic potentials using graphics processing units. *Parallel Comput.* **2009**, *35*, 164−177.
(37) González, M. A.; Abascal, J. L. The shear viscosity of rigid water models. *J. Chem. Phys.* **2010**, *132*, No. 096101.
(38) Song, Y.; Dai, L. L. The shear viscosities of common water models by non-equilibrium molecular dynamics simulations. *Mol. Simul.* **2010**, *36*, 560−567.
(39) Mao, Y.; Zhang, Y. Thermal conductivity, shear viscosity and specific heat of rigid water models. *Chem. Phys. Lett.* **2012**, *542*, 37−41.
(40) Maali, A.; Cohen-Bouhacina, T.; Kellay, H. Measurement of the slip length of water flow on graphite surface. *Appl. Phys. Lett.* **2008**, *92*, No. 053101.
(41) Kannam, S. K.; Todd, B. D.; Hansen, J. S.; Daivis, P. J. Slip flow in graphene nanochannels. *J. Chem. Phys.* **2011**, *135*, No. 016313.
(42) Ko, H. E.; Kwan, S. G.; Park, H. W.; Caron, A. Chemical effects on the sliding friction of Ag and Au (111). *Friction* **2018**, *6*, 84−97.
(43) Priezjev, N. V. Molecular diffusion and slip boundary conditions at smooth surfaces with periodic and random nanoscale textures. *J. Chem. Phys.* **2011**, *135*, No. 204704.

https://dx.doi.org/10.1021/acs.jpcc.0c00854
J. Phys. Chem. C 2020, 124, 11392−11400